JOURNAL OF GEOPHYSICAL RESEARCH, VOL. 116, D20207, doi:10.1029/2011JD015944, 2011

Examination of turbulent entrainment-mixing mechanisms using a combined approach

Chunsong Lu,[1,2] Yangang Liu,[1] and Shengjie Niu[2]

Received 11 March 2011; revised 3 August 2011; accepted 3 August 2011; published 26 October 2011.

[1] Turbulent entrainment-mixing mechanisms are investigated by applying a combined approach to the aircraft measurements of three drizzling and two nondrizzling stratocumulus clouds collected over the U.S. Department of Energy's Atmospheric Radiation Measurement Southern Great Plains site during the March 2000 cloud Intensive Observation Period. Microphysical analysis shows that the inhomogeneous entrainment-mixing process occurs much more frequently than the homogeneous counterpart, and most cases of the inhomogeneous entrainment-mixing process are close to the extreme scenario, having drastically varying cloud droplet concentration but roughly constant volume-mean radius. It is also found that the inhomogeneous entrainment-mixing process can occur both near the cloud top and in the middle level of a cloud, and in both the nondrizzling clouds and nondrizzling legs in the drizzling clouds. A new dimensionless number, the scale number, is introduced as a dynamical measure for different entrainment-mixing processes, with a larger scale number corresponding to a higher degree of homogeneous entrainment mixing. Further empirical analysis shows that the scale number that separates the homogeneous from the inhomogeneous entrainment-mixing process is around 50, and most legs have smaller scale numbers. Thermodynamic analysis shows that sampling average of filament structures finer than the instrumental spatial resolution also contributes to the dominance of inhomogeneous entrainment-mixing mechanism. The combined microphysical-dynamical-thermodynamic analysis sheds new light on developing parameterization of entrainment-mixing processes and their microphysical and radiative effects in large-scale models.

Citation: Lu, C., Y. Liu, and S. Niu (2011), Examination of turbulent entrainment-mixing mechanisms using a combined approach, *J. Geophys. Res.*, *116*, D20207, doi:10.1029/2011JD015944.

1. Introduction

[2] Turbulent entrainment-mixing processes have been regarded as likely candidates for resolving some outstanding problems in cloud physics (e.g., spectral broadening and warm-rain initiation) [*Stommel*, 1947; *Liu and Hallett*, 1998; *Su et al.*, 1998; *Yum and Hudson*, 2001, 2005; *Liu et al.*, 2002a; *Andrejczuk et al.*, 2004; *Lasher-Trapp et al.*, 2005]. The need for improving understanding of entrainment-mixing processes is further reinforced by growing interests in climate-related research and the recognition of the critical role of turbulent entrainment mixing in determining cloud microphysical and radiative properties. Clouds have been thought to be a major source of the uncertainty in climate sensitivity estimates in global climate models (GCMs) because most cloud-related processes occur at subgrid scales of typical GCMs and need to be parameterized [*Cess et al.*, 1989; *Colman*, 2003; *Bony and Dufresne*, 2005; *Stephens*, 2005]. One such subgrid process is the turbulent entrainment-mixing process [e.g., *von Salzen and McFarlane*, 2002].

[3] Turbulent entrainment-mixing processes have been often studied with the so-called homogeneous/inhomogeneous model, but our understanding is still far from complete. Some observations suggested that the entrainment-mixing process was close to homogeneous [e.g., *Jensen et al.*, 1985; *Burnet and Brenguier*, 2007; *Lehmann et al.*, 2009]; others pointed to the inhomogeneous scenario [*Pawlowska et al.*, 2000; *Burnet and Brenguier*, 2007; *Haman et al.*, 2007; *Gerber et al.*, 2008; *Lehmann et al.*, 2009]. However, *Burnet and Brenguier* [2007] pointed out that the entrainment-mixing type is size dependent: A homogeneous entrainment-mixing process may appear to be an inhomogeneous scenario because of spatial averaging of measurements. *Lehmann et al.* [2009] also pointed out that it is unclear whether the entrainment-mixing process is predominantly homogeneous, inhomogeneous, or in between and what the controlling factors are and how they interact. Such an incomplete understanding of different types of entrainment-mixing processes calls for further state-of-the-art observations, because distinguishing

[1]Atmospheric Sciences Division, Brookhaven National Laboratory, Upton, New York, USA.
[2]School of Atmospheric Physics, Nanjing University of Information Science and Technology, Nanjing, China.

0148-0227/11/2011JD015944

homogeneous/inhomogeneous entrainment-mixing processes is key to studying the effect of entrainment-mixing process on warm-rain initiation and cloud-climate feedback. For example, two sensitivity studies using models have recently demonstrated that assuming different types of entrainment-mixing processes (e.g., extreme homogeneous or inhomogeneous entrainment mixing) can significantly affect cloud microphysical properties, cloud radiative properties, and evaluation of aerosol indirect effects [*Grabowski*, 2006; *Chosson et al.*, 2007].

[4] Still less understood is the intimate connection among microphysical, dynamical, and thermodynamic properties associated with different entrainment-mixing processes. More and deeper observational analyses are clearly needed to improve our understanding and quantification of the microphysical-dynamical-thermodynamic connection, which is necessary to improve parameterization of entrainment-mixing processes and their microphysical effects in GCMs, beyond parameterization of the entrainment rate [*Lock*, 2001].

[5] In addition, most of the previous studies have been concerned with maritime clouds and cumulus clouds; continental stratocumulus clouds are relatively underinvestigated. The U. S. Department of Energy's Atmospheric Radiation Measurement (ARM) program conducted an Intensive Observation Period (IOP) of cloud observations at the Southern Great Plains (SGP) site during March 2000. The data collected during this IOP provide a great opportunity to investigate entrainment-mixing processes occurring in midlatitude continental stratocumulus clouds. This study has three primary objectives: (1) to examine turbulent entrainment-mixing processes occurring in the midlatitude continental stratocumulus clouds collected during this IOP in the framework of the homogeneous/inhomogeneous model; (2) to seek the connection among microphysical, dynamical, and thermodynamic properties associated with entrainment-mixing processes; (3) to explore and use an integrative approach that combines analyses of microphysical, dynamical, and thermodynamic relationships.

[6] The rest of the paper is organized as follows. Section 2 briefly describes the IOP experiment, the key instruments on board the Citation aircraft, and the data processing process. Section 3 presents the main results, including the relationship among microphysical properties, cloud dynamical structures, and thermodynamic structures. Concluding remarks are presented in section 4.

2. Description of Cloud IOP and Data

[7] The cloud IOP was conducted by the ARM Research Facility at the SGP site during 1–26 March 2000 and aimed at documenting midlatitude cloud properties for evaluating models and retrieval algorithms. Of particular relevance to this work are the 12 flights taken with the Cessna Citation research aircraft of the University of North Dakota. Cloud droplet and drizzle size distributions were measured with a Particle Measuring Systems (PMS) Forward Scattering Spectrometer Probe (FSSP-100) and an optical array probe (1D-C), respectively. The FSSP sizes and counts cloud droplets in 15 bins, with bin centers from 5.3 to 59.8 μm in diameter; the 1D-C probe has 30 bins with bin centers from 24.1 to 600 μm in diameter. Measurements of both instruments are corrected with standard procedures. Briefly, corrections to particle concentrations from the FSSP are applied to account for probe activity and coincidence (electronic dead time) [*Baumgardner et al.*, 1985] and for variations in the effective beam diameter [*Dye and Baumgardner*, 1984]. Corrections to particle sizes to account for electronic response time and beam inhomogeneity follow the method of *Baumgardner and Spowart* [1990]. The sizing correction scheme redistributes the counts, and the bin widths are adjusted to account for ambiguities in the Mie scattering curve. Particle concentrations and sizes from the 1D-C are corrected for aircraft speed and electronic delays after the method by *Baumgardner* [1987]. The aircraft was also mounted with a Cloud Particle Imager (CPI) manufactured by the Stratton Park Engineering Company; images of cloud particles collected with the CPI are used, together with air temperature, to ascertain the clouds analyzed are liquid-water clouds. Air temperature, air pressure, and dew point were measured with Rosemount model 102, Rosemount model 1201F1, and EG&G model 137 probes, respectively. Relative humidity was calculated based on the dew point, air temperature, and air pressure. True air speed was measured by Rosemount 1221F. The turbulent dissipation rate was derived from the true airspeed using a structure function (see Appendix A for details). Vertical wind speed was calculated based on the wind equations described by *Khelif et al.* [1999] with the data observed by Validyne P40D and Applanix Position and Orientation System (POS). The 1 Hz data are used in this study.

[8] This paper is mainly concerned with nondrizzling clouds and nondrizzling flight horizontal legs in drizzling clouds; thus the key microphysical properties used in this study, including liquid water content (LWC), droplet number concentration (N), and volume-mean radius (r_v), are calculated from the FSSP-measured droplet size distribution. The 1D-C measurements are mainly used for determining whether or not a flight leg was drizzling. A leg was considered as drizzling if the 1D-C probe showed the existence of drizzle drops with diameters >50 μm and there were drops of ~50 μm diameter in the FSSP-measured droplet size distributions. Similarly, a cloud was considered as drizzling if there was at least one drizzling leg. A cloud record is defined by the criteria of $N > 10$ cm^{-3} and LWC > 0.001 g m^{-3} [*Deng et al.*, 2009; *Zhang et al.*, 2011]. Both thresholds for N and LWC are introduced to eliminate the cloud droplet size distributions that are probably composed of large aerosols instead of cloud droplets.

[9] A total of 12 cases were measured during the cloud IOP, including stratocumulus, altocumulus, and cirrus. This paper focuses on five warm stratocumulus cases that either had cloud top temperatures above 0°C or no ice crystals based on the CPI particle images (these ice-free clouds are referred to as warm clouds throughout this paper). Among these five cases, two cases (3, 19 March 2000) were nondrizzling and the other three (17, 18, 21 March, 2000) were drizzling. To minimize the effect of the collision and coalescence process in drizzling cases, only nondrizzling flight legs are examined in this study.

[10] A total of 16 nondrizzling horizontal flight legs that satisfy these conditions are identified and analyzed using a combined approach to be detailed later in section 3. To ensure sufficient statistics, these selected flight legs had a

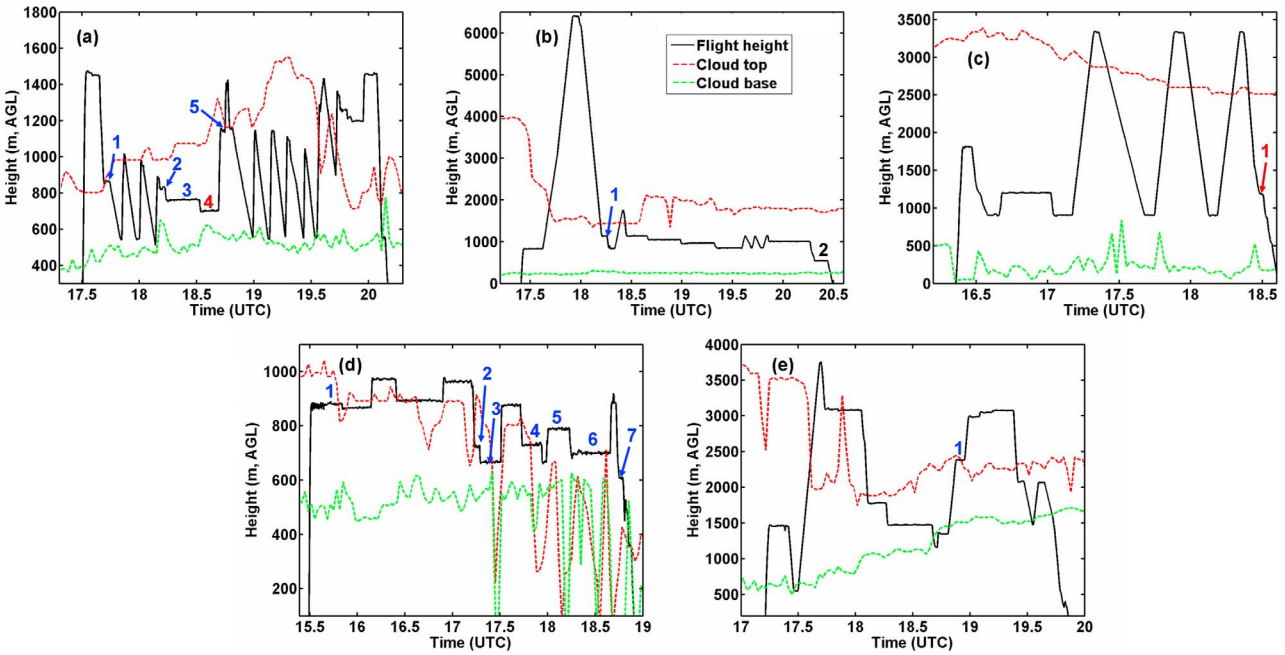

Figure 1. Temporal evolutions of aircraft height, cloud top and base in the five cases at Southern Great Plains (SGP) site during the five cases: (a) 3 March 2000, (b) 17 March 2000, (c) 18 March 2000, (d) 19 March 2000, (e) 21 March 2000. The numbers in the figures are horizontal leg numbers, and their different colors represent different mechanisms. Blue, extreme inhomogeneous entrainment-mixing mechanism; red, inhomogeneous entrainment mixing with subsequent ascent; black, homogeneous entrainment-mixing mechanism.

horizontal length of at least 12 km and 15 cloud droplet size distributions. Figure 1 summarizes these legs along with the dominant entrainment-mixing mechanisms. For convenience, a leg number is designated for every flight leg of each case, and different colors represent different entrainment-mixing mechanisms in this figure. The entrainment-mixing mechanisms shown here are based on the microphysical analysis only (see section 3.1 for details).

[11] Also shown in Figure 1 are the cloud top and base according to the ARM Active Remotely Sensed Cloud Locations (ARSCL) Value Added Product (VAP) as references for judging the leg position in the corresponding clouds. It is noteworthy that because of the different sampling areas of cloud in the measurements of radar, ceilometer, and aircraft, the radar-measured cloud top and ceilometer-derived base might not well represent the cloud area where the aircraft was penetrating, especially when the cloud was dissipating and shallow, such as the 19 March 2000 case [*Dong et al.*, 2002], in which sometimes the cloud top was shown incorrectly lower than the cloud base (Figure 1d). However, the information on the cloud top and base still provided valuable references for analysis.

3. Methodology and Results

3.1. Microphysical Results

3.1.1. Homogeneous/Inhomogeneous Model

[12] The basic understanding of the connection between cloud microphysical relationships and different types of entrainment-mixing processes in the framework of the homogeneous/inhomogeneous entrainment-mixing model has been largely built on the classical work presented by *Baker and Latham* [1979] and *Baker et al.* [1980]. According to this model, the microphysical relationship associated with different entrainment-mixing processes can be classified into three major types, and is briefly discussed below.

[13] The first type is the homogeneous entrainment-mixing mechanism. Under this mechanism, all cloud droplets are exposed to the same environmental conditions and evaporate at the same time. Thus r_v and N are anticipated to be positively correlated. The extreme homogeneous scenario in which N remains unchanged while droplets evaporate and shrink has been often cited as a typical example of homogeneous mixing, especially in parameterization of entrainment-mixing processes for large-scale models [*Grabowski*, 2006; *Chosson et al.*, 2007].

[14] The second type is the so-called extreme inhomogeneous entrainment-mixing mechanism. It proceeds in two steps: All droplets surrounding the entrained dry-air parcel first evaporate to just saturate the parcel; and then mixing between this parcel and the remaining part of cloud dilutes the cloud. Under such conditions, r_v changes slightly as N decreases because of evaporation.

[15] The third type is a continuation of the extreme inhomogeneous mixing that can be described as follows. If the diluted parcel after the extreme inhomogeneous entrainment-mixing process is lifted upward again, the big droplets in this parcel are expected to grow faster than those in other undiluted parcels because of less competition for water vapor. Under such conditions, r_v is negatively correlated to N. To distinguish this from the commonly cited extreme inhomogeneous entrainment mixing, the type that exhibits a negative

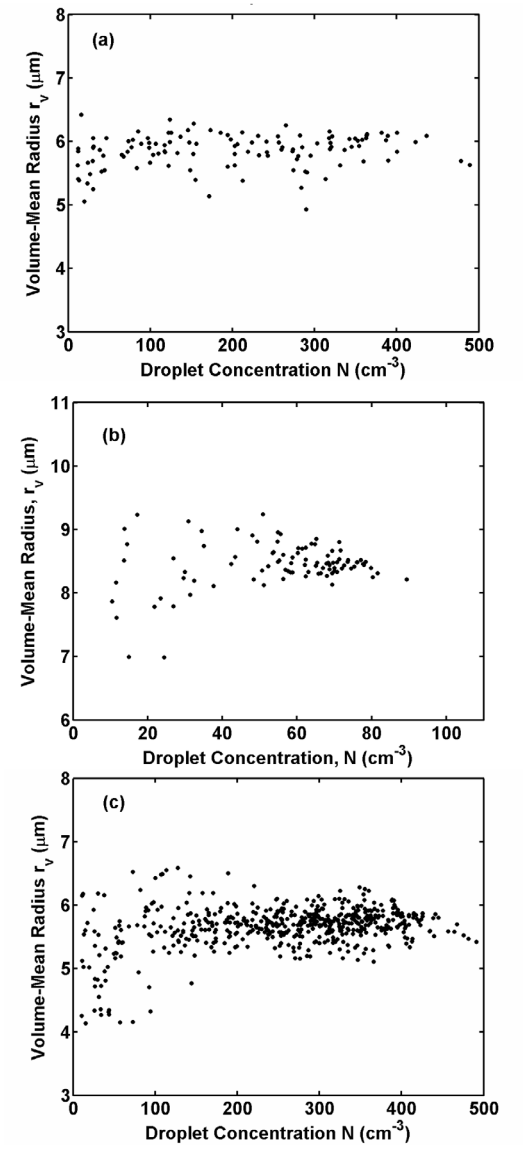

Figure 2. Relationship between the volume-mean radius (r_v) and the cloud droplet number concentration (N) along (a) Leg 2 of the 19 March 2000 case, (b) Leg 1 of the 17 March 2000 case, and (c) Leg 3 of the 03 March 2000 case, dominantly affected by the extreme inhomogeneous entrainment-mixing process.

r_v-N correlation is herein termed as inhomogeneous entrainment mixing with subsequent ascent.

3.1.2. Microphysical Analysis

[16] Based on the above qualitative analysis, the r_v-N relationship is expected to have distinct characteristics for different types of entrainment-mixing processes. This unique feature has been widely employed to identify entrainment-mixing mechanisms in numerous previous studies [e.g., *Pawlowska et al.*, 2000; *Burnet and Brenguier*, 2007; *Lehmann et al.*, 2009] and is used in this paper. Another reason for focusing on the r_v-N relationship is its close link to the parameterization of effective radius and study of aerosol indirect effects [*Shao and Liu*, 2006; *Kim et al.*, 2008]. We have analyzed the r_v-N relationships of all 16 nondrizzling legs, and we discuss the main results below.

[17] The extreme inhomogeneous entrainment-mixing signature was found for 13 out of 16 flight legs observed during this IOP. Figure 2 shows three representative examples. Figure 2a displays the result for Leg 2 of the 19 March 2000 case. According to *Dong et al.* [2002], this cloud was at its dissipating stage and the measurement was carried out around the cloud top (see also Figure 1d). This cloud was unique in that all seven legs exhibit similar features as exemplified here. Second, two nondrizzling legs in the drizzling clouds (Leg 1 of the 17 March 2000 case and Leg 1 of the 21 March 2000 case) were also mainly affected by the extreme inhomogeneous entrainment-mixing process; Figure 2b shows the result for Leg 1 of the 17 March 2000 case as an example. As indicated in Figures 1b and 1e, these legs were both sampled near the cloud tops. Previous studies have also documented the occurrence of the extreme inhomogeneous entrainment-mixing mechanism near cloud tops [*Pawlowska et al.*, 2000; *Burnet and Brenguier*, 2007; *Lehmann et al.*, 2009], especially when the cloud was dissipating [*Lehmann et al.*, 2009]. It is intriguing to note that the extreme inhomogeneous entrainment-mixing mechanism also occurred along Legs 2 and 3 in the middle level of the 03 March 2000 case (e.g., Leg 3, Figure 2c).

[18] Two legs were found to be predominantly affected by the inhomogeneous entrainment mixing with subsequent ascent (Figure 3) in two different conditions: (1) Leg 4 was in a nondrizzling cloud (the 3 March 2000 case) and (2) Leg 1 was a nondrizzling leg in a drizzling cloud (the 18 March 2000 case). What was particularly interesting was that the two legs exhibited significant differences in their ranges of N. The majority of data points along Leg 4 of the 3 March 2000 case had N larger than 100 cm^{-3} while the N varied from ~20 to 100 cm^{-3} along Leg 1 of the 18 March 2000 case. Inspection of Figures 1a and 1c indicates that the two legs were both located in the middle of the clouds. Furthermore, such a scenario in which larger droplets are accompanied by smaller N was found in previous observations [e.g., *Siebert et al.*, 2006; *Lehmann et al.*, 2009]. The numerical simulations by *Lasher-Trapp et al.* [2005] and *Krueger* [2008] also showed that the ascending mixed parcels could produce larger droplets than during an adiabatic ascent.

[19] Only one flight leg as a whole (Leg 2 of the 17 March 2000 case) exhibited some microphysical feature of the homogeneous entrainment-mixing process with a correlation coefficient of 0.15 between N and r_v (Figure 4, especially when droplet concentration <~200 cm^{-3}). This leg lay in the lower part of the cloud, which seemed consistent with previous studies that have suggested that homogeneous mixing often occurs in less-diluted regions such as a growing core [*Burnet and Brenguier*, 2007; *Lehmann et al.*, 2009].

[20] It is worth mentioning that the emphasis of the above analysis was on leg averages. In fact, for some legs, the divisions between different types were not as sharp as described in the qualitative classification, and different types sometime coexisted along the same leg (more discussion on this mixture behavior is deferred to section 3.2.3).

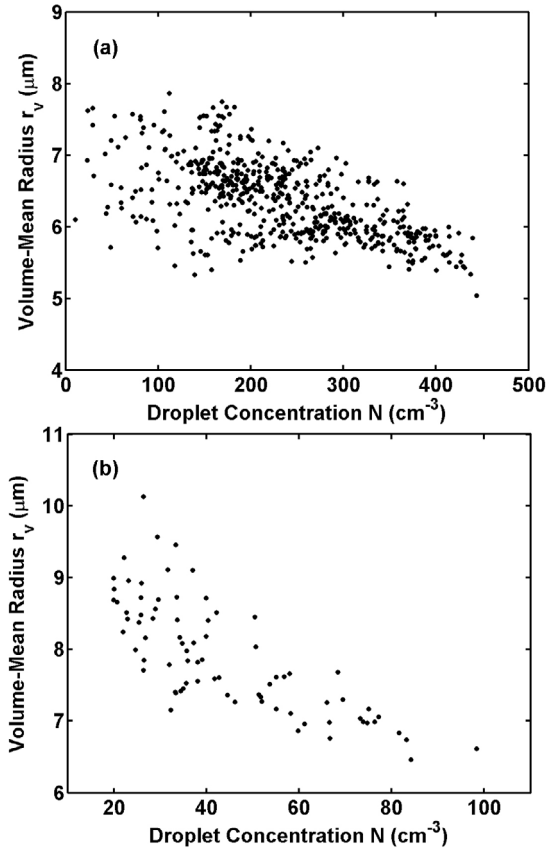

Figure 3. Relationship between the volume-mean radius (r_v) and the cloud droplet number concentration (N) along (a) Leg 4 of the 3 March 2000 case, and (b) Leg 1 of the 18 March 2000 case, dominantly affected by the inhomogeneous entrainment-mixing with subsequent ascent.

3.2. Dynamical Analysis and Transition Scale Number

3.2.1. Theoretical Formulation

[21] Except for the microphysical relationship between N and r_v, the partition between homogeneous and inhomogeneous entrainment-mixing processes has been often based on two characteristic time scales, evaporation time τ_{evap} and turbulent mixing time τ_{mix}, since the pioneering work by *Baker and Latham* [1979] and *Baker et al.* [1980]. The evaporation time expresses the time needed for a population of droplets with a mean radius r_m to evaporate in a subsaturated environment and is given by

$$\tau_{\text{evap}} = -\frac{r_m^2}{2As}, \tag{1}$$

where A is a function of air pressure and temperature and s the supersaturation [e.g., *Rogers and Yau*, 1989] (see Appendix B for details). The negative sign is introduced to denote the fact that s is negative in a subsaturated environment. The turbulent mixing time represents the time needed for complete homogenization of a volume of a linear size L through the process of turbulent diffusion and is given by

$$\tau_{\text{mix}} \sim \left(\frac{L^2}{\varepsilon}\right)^{1/3}, \tag{2}$$

where ε is the eddy dissipation rate of turbulent kinetic energy [*Baker et al.*, 1984; *Burnet and Brenguier*, 2007; *Wyngaard*, 2010]. The occurrence of homogeneous or inhomogeneous mixing can be discerned from the ratio of the two characteristic time scales defined as the Damköhler number (Da) or its reciprocal [*Siebert et al.*, 2006; *Burnet and Brenguier*, 2007; *Jeffery*, 2007; *Andrejczuk et al.*, 2009]:

$$Da = \frac{\tau_{\text{mix}}}{\tau_{\text{evap}}}. \tag{3}$$

Despite its popularity, this approach suffers from a serious shortcoming: The value of L used in the calculations of τ_{mix} and Da is ambiguous [*Lehmann et al.*, 2009]. Major progress was achieved lately by *Lehmann et al.* [2009] to overcome this difficulty by introducing the concept of transition length (L^*) as the value of L that corresponds to the unit Da. The substitution of $Da = 1$ and equation (2) into equation (3) leads to the expression for the transition length:

$$L^* = \varepsilon^{1/2}\tau_{\text{react}}^{3/2}, \tag{4}$$

where reaction time τ_{react} is defined as either the time when the droplets have completely evaporated or the time at which the relative humidity has reached 99.5% ($s > -0.005$). Note that τ_{react} is used instead of τ_{evap} to relax the limited assumption that the supersaturation s is a constant for the calculation of $\tau_{\text{evap.}}$ See Appendix B for details about the calculation of τ_{react}. *Lehmann et al.* [2009] argued that if L^* falls within the turbulent inertial subrange, after a blob of size L_E of subsaturated air is entrained into a cloud, all eddies of size L in the range of $L^* < L < L_E$ will experience inhomogeneous entrainment-mixing processes, whereas eddies smaller than L^* will mix homogeneously.

[22] Following *Lehmann et al.* [2009] and recognizing that the lower end of the turbulent inertial subrange is represented by the Kolmogorov length scale η, here we further introduce a new dimensionless number, called the scale number (N_L) and defined as the ratio of L^* to η:

$$N_L = \frac{L^*}{\eta}, \tag{5}$$

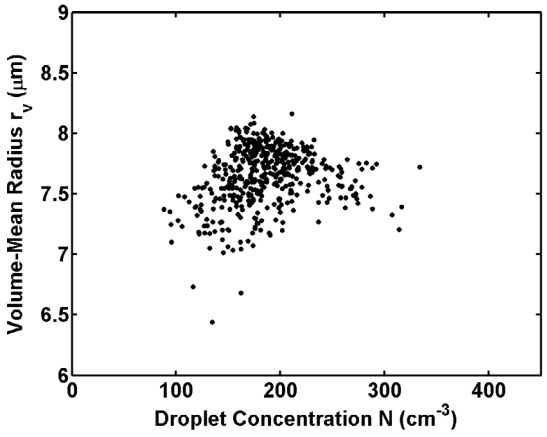

Figure 4. Relationship between the volume-mean radius (r_v) and the droplet number concentration (N) along Leg 2 of the 17 March 2000 case, dominantly affected by the homogeneous entrainment-mixing process.

Table 1. Air Temperature, Relative Humidity and Water Vapor Mixing Ratio Above the Cloud Top in the Five Cases

Case	Type	Temperature (°C)	Relative Humidity (%)	Water Vapor Mixing Ratio (g kg^{-1})
3 March 2000	Non-drizzling	0.5	60.8	2.9
17 March 2000	Drizzling	−5.0	61.6	2.5
18 March 2000	Drizzling	−3.1	38.1	1.7
19 March 2000	Non-drizzling	2.3	42.4	2.2
21 March 2000	Drizzling	−0.9	26.7	1.5

where η is given by

$$\eta = \left(\frac{\upsilon^3}{\varepsilon}\right)^{1/4}, \quad (6)$$

and ν is the kinematic viscosity [*Wyngaard*, 2010] (see Appendix B for details).

[23] Similar to L^*, N_L is a dynamical measure of the degree of the homogeneous or inhomogeneous entrainment-mixing process, but accounts for both L^* and η: the larger the N_L, the stronger the homogenous entrainment-mixing process and the weaker the inhomogeneous entrainment-mixing process.

3.2.2. Leg-Averaged Scale Number

[24] To examine the applicability of this idea and make a connection to the microphysical results presented in section 3.1, we have computed L^*, η, and N_L for all the legs. In the calculation, the air with temperature and moisture in the environment just above the cloud tops (Table 1) is assumed to be entrained into the clouds. Basically, these values are based on the vertical profiles of temperature, relative humidity, and water vapor mixing ratio along the first vertical penetrations of clouds at the beginning of flights. A similar method was used by *Lehmann et al.* [2009] in their cumulus study. If such a penetration is not available, as, for example, in the 19 March 2000 case, a penetration in the middle of the flight is used.

[25] Figure 5 shows the N_L for all the legs, where the blue, red, and black colors represent the extreme inhomogeneous mixing, inhomogeneous mixing with subsequent ascent, and homogeneous mixing as identified by the microphysical analysis, respectively.

[26] The only leg (Leg 2 of the 17 March 2000 case) dominated by the homogeneous entrainment-mixing process according to the microphysical analysis conspicuously had the largest N_L of 53.7, while other legs affected by the inhomogeneous entrainment-mixing process had smaller N_L. *Lehmann et al.* [2009] pointed out that the homogeneous mixing process was more likely to occur in the vicinity of the cloud core of cumulus, where vertical velocity, temperature, ε, N, and LWC were positively correlated, while the inhomogeneous entrainment-mixing mechanism dominated in the more-diluted cloud regions. The five cases presented here did not have such cloud cores; positive correlations among vertical velocity, temperature, ε, N, and LWC were not identified, implying that these clouds were aged and not actively growing. However, the comparison between Leg 2, affected by the homogeneous entrainment-mixing process in the 17 March 2000 case, and Leg 1, dominated by the inhomogeneous entrainment-mixing process in the same case, could still provide some hints to further examine the causes of the two mechanisms (Figure 6). The reason for choosing Leg 1 of the 17 March 2000 case representing the inhomogeneous entrainment-mixing mechanism was that these two legs were in the same case and were expected to have a similar environment. Thus, we can focus on the effect of entrainment mixing on the microphysical relationships to the greatest extent.

[27] It is evident that the vertical velocity was mainly positive along Leg 2 but negative along Leg 1. Moreover, the ε, N, LWC, and N_L were much larger along Leg 2 than along Leg 1. Therefore, compared with Leg 1, Leg 2 was closer to the "cloud core" with less dilution and Leg 1 had

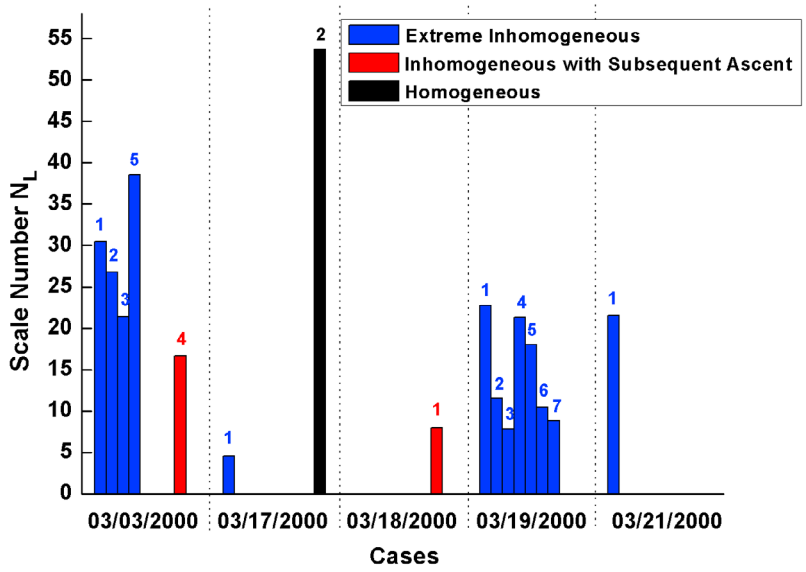

Figure 5. Bar plot for the average scale number (N_L) along different legs in the five cases.

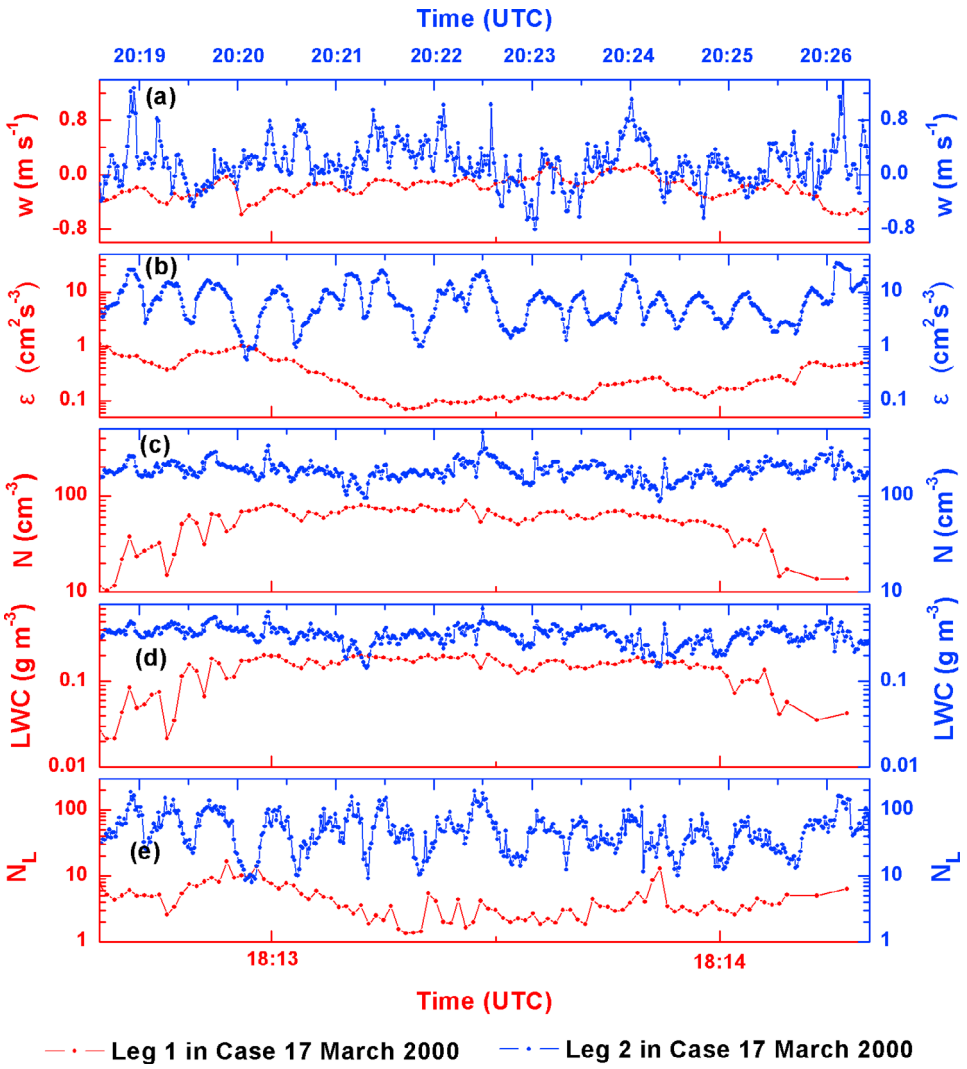

Figure 6. (a) Temporal variations of vertical velocity (w), (b) dissipation rate (ε), (c) number concentration (N), (d) liquid-water content (LWC), (e) scale number (N_L) along Leg 1 and Leg 2 of the 17 March 2000 Case. The dots represent the 1 Hz data.

experienced extensive dilution. This was consistent with the aforementioned conclusion given by *Lehmann et al.* [2009]. In addition, if a blob with size L_E was assumed to be entrained from above the cloud top and moved downward, the parcel would be stretched into smaller blobs. The more the blob moved downward, the smaller the size that would be obtained [*Krueger*, 1993]. The height of Leg 2 was lower than that of Leg 1; therefore Leg 2 could have smaller blobs, increasing the probability of their sizes being located in the range from η to L^*. This could be another reason for the homogeneous entrainment-mixing process along Leg 2.

[28] Except for the two legs in the 17 March 2000 case, which had the largest and smallest N_L (Figure 5), the correspondence between the analyses of microphysical relationship and scale number was not that obvious in their relations to entrainment-mixing types along the legs with intermediate values of N_L; a careful comparison of the results for the two legs dominantly affected by the inhomogeneous mixing with subsequent ascent to other legs suggests that these two legs shared similar scale numbers with some other legs affected by the extreme inhomogeneous entrainment-mixing mechanism. Although the samples here are too limited to be conclusive, this phenomenon should be emphasized and warrants substantiation. The reason for such a lack of unique one-to-one correspondences between scale number and microphysical relationships could be that dynamical analysis through scale number here or Damköhler number [*Siebert et al.*, 2006; *Burnet and Brenguier*, 2007; *Jeffery*, 2007; *Andrejczuk et al.*, 2009] or transition length [*Lehmann et al.*, 2009] in previous studies can distinguish homogeneous and inhomogeneous entrainment-mixing processes, but cannot further distinguish the two types of inhomogeneous mixing processes: extreme scenario and inhomogeneous mixing with subsequent ascent. Thus such a lack of unique one-to-one correspondences between microphysical and dynamical properties highlights the importance of combined microphysical and dynamical analyses in the investigation of turbulent entrainment-mixing processes.

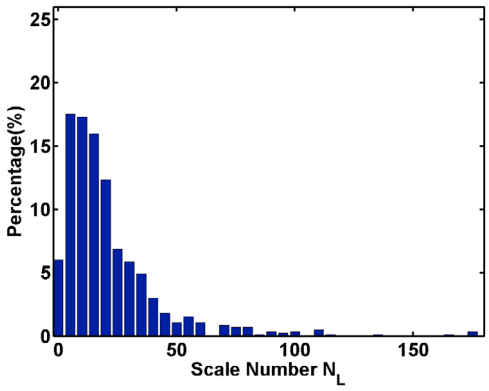

Figure 7. Probability density function of 1 Hz scale number (N_L) along Leg 3 of the 3 March 2000 case.

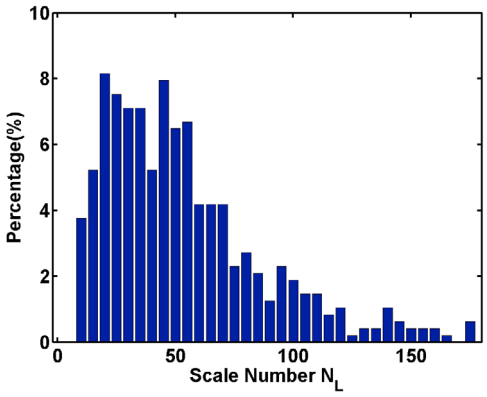

Figure 8. Same as Figure 7 but for Leg 2 of the 17 March 2000 case.

3.2.3. A Probabilistic View of the Scale Number

[29] *Lehmann et al.* [2009] obtained a transition scale L^* that starts to favor homogeneous mixing at approximately 10 cm, which is close to leg-averaged value $L^* = 7.4$ cm for Leg 2 of the 17 March 2000 case; L^* of ~10 cm means N_L of ~50 for a typical value of η ~2 mm. Except for the leg-averaged N_L, the further examination of spatial distribution of N_L is necessary because N_L along one leg is not uniform. The spatial distribution of N_L along one leg is expected to be responsible for the simultaneous occurrence of different types of entrainment-mixing mechanisms, as mentioned in section 3.1. For example, Figure 7 shows the probability density function of N_L (1 Hz) along Leg 3 of the 3 March 2000 case; it is clear that most N_L values were in the range of 5–20, corresponding to the dominance of the extreme inhomogeneous entrainment-mixing mechanism; however, there were still some values larger than 50 or even 150, giving a sign of the occurrence of homogeneous entrainment-mixing process, which was supported by the weak positive correlation between r_v and N for $N <$ ~100 m along this leg (Figure 2c). Similarly, for Leg 2 of the 17 March 2000 case, although it was dominantly affected by the homogeneous entrainment-mixing mechanism, the negative correlation of r_v versus N for $N >$ ~200 cm^{-3} (Figure 4) showed the occurrence of the inhomogeneous entrainment-mixing process, which could be related to the existence of small N_L (Figure 8). The wider distribution of N_L from smaller to larger than 50 was a common phenomenon; only Leg 1 in the 17 March 2000 case had maximum N_L smaller than 50. The wider distribution of N_L could be further augmented by Figure 9 in that the standard deviation of N_L generally increased with its mean for all the legs in general. Therefore, even a dominance of one specific entrainment-mixing mechanism could not completely rule out the occurrence of other mechanisms.

3.3. Thermodynamic Structure

[30] To examine the relevance of cloud thermodynamic structure to entrainment-mixing mechanisms, this section examines the relationship of air temperature to N. The results show that all 16 legs exhibited more or less negative correlations between the temperature and N, with different magnitudes of correlation and slopes, as exemplified in Figure 10 for Leg 4 of the 3 March 2000 case, Legs 1 and 2 of the 17 March 2000 case, and Leg 2 of the 19 March 2000 case. At first glance, this negatively correlated relationship seemed to contradict the evaporation of droplets associated with entrainment-mixing processes that likely lowered both the temperature and N [e.g., *Lewellen and Lewellen*, 1998; *Yamaguchi and Randall*, 2008]. On the other hand, *Haman et al.* [2007] showed that filaments of dry and cloudy air of sizes smaller than 10 cm were ubiquitous in clouds, and the inevitable averaging of different filaments during the sampling process could cause such a negative correlation. For this study, the 1 Hz sampling interval corresponded to a spatial distance of about 100 m, and thus any measurement was an average that lumped together unsaturated droplet-free air and cloudy air of different filaments of sizes smaller than 100 m [*Wang et al.*, 2009]. The effect of the filament structure on the relationship between temperature and N is schematically illustrated by Figure 11. Because of evaporative cooling, uniform filaments containing liquid water after mixing are cooler than unmixed clouds (see Figure 14 of *Haman et al.* [2007] for details); therefore, the temperature in cloudy Filaments A and B could be lower, but the

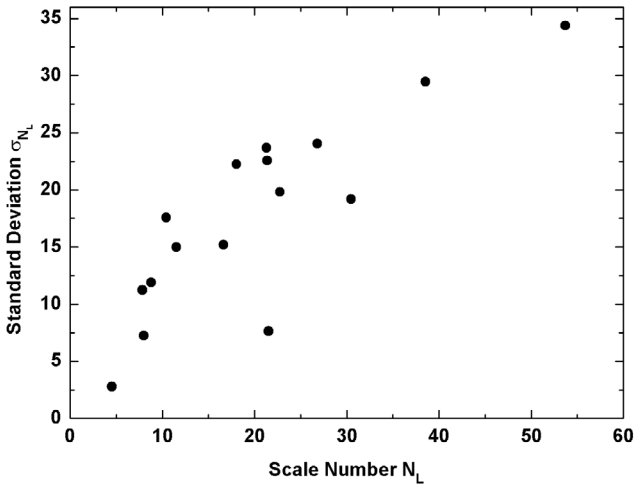

Figure 9. Relationship between the leg mean scale number N_L and the corresponding standard deviation.

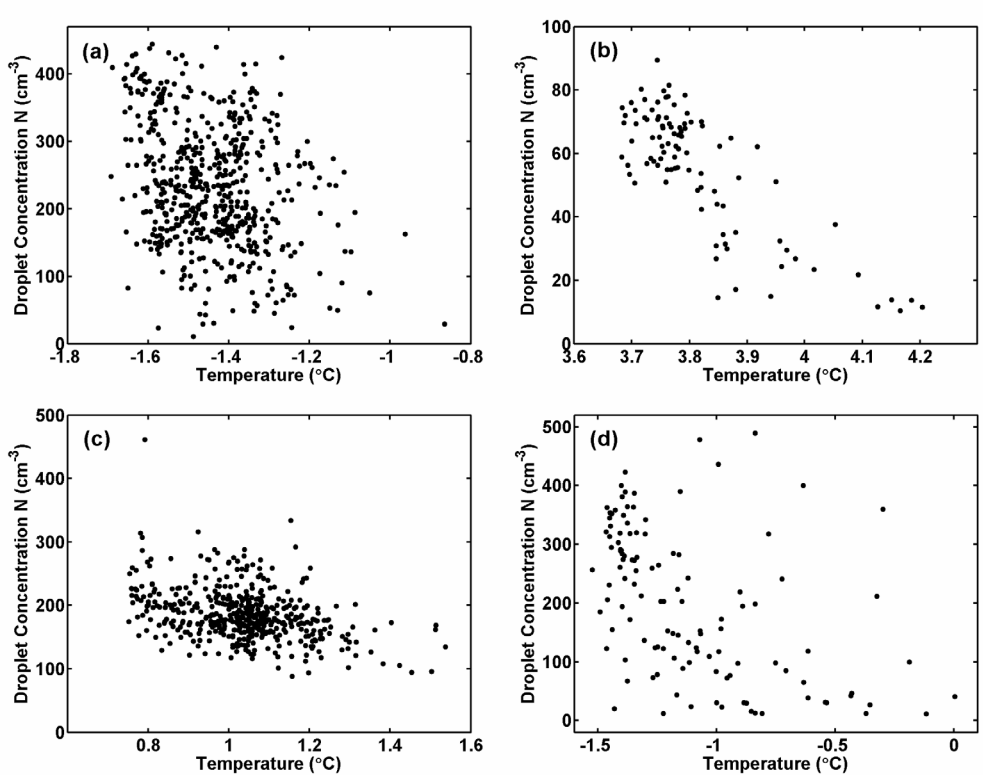

Figure 10. Relationships between the droplet number concentration (N) and air temperature along (a) Leg 4 of the 3 March 2000 case, (b) Leg 1 of the 17 March 2000 case, (c) Leg 2 of the 17 March 2000 case, and (d) Leg 2 of the 19 March 2000 case.

warm and dry cloud-free air in the mixture could contribute to the higher average temperature and lower N.

[31] To some degree, the filament structures could also contribute to the observed small variation in r_v but large variation in N, which is identified as the microphysical signature of the extreme inhomogeneous entrainment-mixing mechanism [*Baker et al.*, 1984; *Burnet and Brenguier*, 2007; *Haman et al.*, 2007; *Andrejczuk et al.*, 2009]. However, by comparing the results derived from model simulations and observations, *Burnet and Brenguier* [2007] also pointed out that proper physical processes could lead to the extreme inhomogeneous mixing as well. Our analysis of the transition scale number in the last subsection affirms their finding. This relevance of microphysical relationship to thermodynamic structure further highlights the need for an approach that combines analyses of microphysical, dynamical, and thermodynamic properties.

4. Concluding Remarks

[32] By use of a combined analysis of microphysical relationship and dynamical and thermodynamic structures, different types of entrainment-mixing mechanisms are examined for the microphysical, dynamical, and thermodynamic signatures. Data on 16 nondrizzling horizontal flight legs in five warm continental stratocumulus clouds collected during the March 2000 cloud IOP conducted at the SGP site are analyzed.

[33] The analysis of the microphysical relationship shows that, on average, the extreme inhomogeneous entrainment-mixing mechanism with the relationship of a constant volume-mean radius versus varying droplet concentrations was dominant, and 13 out of 16 flight legs were mainly influenced by this type. Although most legs thus affected were near cloud tops, as reported in many previous studies, two legs in the middle level of a cloud were found to exhibit the microphysical signature of this type. This result suggests

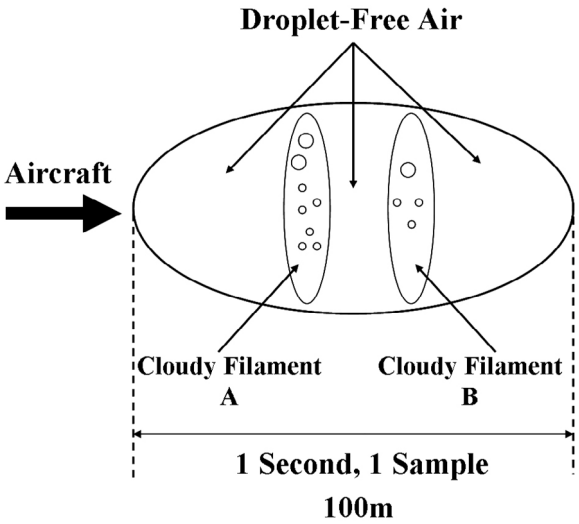

Figure 11. Schematic illustration of the filament structure of a sample as collected by the instrumented aircraft. The circles in Filaments A and B represent cloud droplets.

that the entrained dry air at the cloud top penetrated deeper (200–300 m) into clouds under some conditions and resulted in extreme inhomogeneous entrainment mixing. Two legs were found to exhibit a negative correlation between volume-mean radius and droplet concentration, a microphysical signature of inhomogeneous entrainment mixing with subsequent ascent. Only one leg was weakly influenced by the homogeneous entrainment-mixing mechanism with a positive correlation between volume-mean radius and droplet concentration.

[34] A new dimensionless number called the scale number is introduced to characterize the dynamical properties of different types of entrainment-mixing processes. It is argued from theoretical analysis of major characteristic scales (turbulent mixing scale, droplet reaction scale, and the Kolmogorov microscopic scale) that the scale number can be utilized as a dynamical measure of the chance for the occurrence of homogeneous entrainment-mixing process: The larger the scale number, the higher the chance for homogeneous mixing to occur. Similarly, a smaller scale number means a higher probability of the inhomogeneous entrainment-mixing mechanism. Observational analysis of scale number for all the flight legs reveals three points. First, the data support our theoretical projection that among all the legs examined, the leg with the microphysical signature of homogeneous mixing had the largest scale number, and the least scale number tended to be associated with the leg dominantly affected by the extreme inhomogeneous mixing. Second, there was no one-to-one correspondence between the microphysical signature and the scale number for those legs with intermediate values of the scale number; a similar scale might correspond to microphysical signatures of either the extreme inhomogeneous entrainment mixing or the inhomogeneous entrainment mixing with subsequent ascent. Finally, a more complete characterization of entrainment-mixing processes demands a probabilistic description, which further shows that different entrainment-mixing mechanisms tended to occur simultaneously and one dominant mechanism could not rule out the occurrence of the others. The last two points highlight the importance of integrating the microphysical and dynamical analyses in discerning different types of entrainment-mixing processes.

[35] Thermodynamic analysis indicates the omnipresence of a negatively correlated relationship between air temperature and droplet number concentration along all legs in the five cases. It is argued that this phenomenon confirmed indirectly what was hypothesized by *Burnet and Brenguier* [2007]: A cloud (leg) consists of various cloudy and droplet-free filaments; a sample collected over a 1 s time interval, which spans about 100 m in space, represents an average of many cloudy and droplet-free filaments; and the sampling average of different filaments tends to produce a large variation of droplet concentrations without significant change of the droplet size during sampling, and thus is at least partly responsible for the dominance of the extreme scenario.

[36] Altogether, the results derived from our combined analysis suggest that although each analysis is individually useful for studying entrainment-mixing processes, a complete characterization often requires integrative application of the three approaches. Furthermore, the combined approach sheds new light on the microphysical-dynamical-thermodynamic connection, which is essential for developing microphysical parameterization in relation to different entrainment-mixing processes for use in large-scale models.

[37] Several points are noteworthy. First, this paper examines entrainment-mixing processes in the framework of the homogeneous/inhomogeneous mixing model pioneered by Baker and her coworkers, without invoking other models such as the entity-type entrainment mixing [*Telford and Chai*, 1980; *Telford*, 1996] and internal mixing [*Hudson and Yum*, 1997]. Related subjects also include clustering [*Kostinski and Shaw*, 2001], turbulence fluctuations [*Liu et al.*, 2002b], and cloud inhomogeneity [*Davis et al.*, 1999]. Second, our results suggest that the common classification of three qualitative types is an oversimplification; a quantitative continuum for each qualitative type likely exists. However, because of limited data sets, the results cannot be considered conclusive; more and further investigations are necessary to substantiate our findings. For example, to further explore the behavior in clouds, especially in the filament cloud area, high-resolution measurements are necessary [*Malinowski and Pawlowska*, 1989; *Grabowski and Pawlowska*, 1993; *Haman et al.*, 2007]. Third, albeit in its infancy, the necessity of seeking and quantifying the connection among microphysics, dynamics, and thermodynamics regarding entrainment-mixing processes cannot be overemphasized; both theoretical analyses and high-resolution numerical simulations of the scale number are under way, seeking physics-based parameterizations of entrainment-mixing processes and their microphysical and radiative effects in large-scale models.

Appendix A: Calculation of Turbulent Dissipation Rate

[38] Turbulent dissipation rate is calculated from measurements of an aircraft's true airspeed U [*Poellot and Grainger*, 1991]:

$$\varepsilon = \left(\frac{D}{C}\right)^{3/2} \frac{1}{\delta x}, \tag{A1}$$

where C is Kolmogorov's constant (1.77), δx is the lag distance between samples, and D is a structure function:

$$D = (U(x) - U(x + \delta x))^2. \tag{A2}$$

U was measured at a frequency of 24 Hz; a moving average of five samples was performed to eliminate the transducer noise. The 24 Hz structure function is calculated by taking the square of the difference of the smoothed U with a lag of 12 samples (0.5 s); the lag distance (δx) is calculated by multiplying the average U over a 0.5 s period by the time increment (0.5 s), which is around 50 m. The 24 Hz dissipation rate is calculated with equation (A1). In this paper, the 24 Hz values are further averaged to 1 Hz to reduce noise and to be consistent with size distribution measurements. Because it provides much needed high-frequency data on the dissipate rate, a similar method has been widely used in previous studies [e.g., *Labitt*, 1981; *Paluch and Baumgardner*, 1989; *Gultepe and Starr*, 1995; *Meischner et al.*, 2001; *Cho et al.*, 2003].

[39] It is noteworthy that equation (A1) strictly holds when the turbulence is isotropic and the lag distance is within the inertial subrange. A deviation from these assumptions can result in errors in thus calculated dissipation rates. *Meischner et al.* [2001] examined the dependence of dissipation rate on lag distance with a similar calculation method of dissipation rate (structure functions of longitudinal and normal components of true airspeed instead of true airspeed). *Cho et al.* [2003] also discussed the dependence of dissipation rate on lag distance.

Appendix B: Calculation of Scale Number (N_L)

[40] The scale number (N_L) is defined as the ratio of L^* to the Kolmogorov microscale η:

$$N_L = L^*/\eta. \tag{B1}$$

The η is given by

$$\eta = \left(\frac{\upsilon^3}{\varepsilon}\right)^{1/4}, \tag{B2}$$

where ν is the kinematic viscosity [*Wyngaard*, 2010].

[41] The transition length (L^*) is calculated using the same approach presented by *Lehmann et al.* [2009]. Briefly, L^* is given by

$$L^* = \varepsilon^{1/2}\tau_{\text{react}}^{3/2}. \tag{B3}$$

The reaction time τ_{react} is calculated through the combination of equations (B4) and (B5) when a population of droplets completely evaporate (mean radius $r_m = 0$) in a subsaturated environment or relative humidity reaches 99.5% (supersaturation $s > -0.005$):

$$\frac{dr_m}{dt} = A\frac{s}{r_m} \qquad A = \frac{1}{\left[\left(\frac{L_h}{R_vT} - 1\right)\frac{L_h\rho_L}{KT} + \frac{\rho_L R_v T}{De_s(T)}\right]}, \tag{B4}$$

$$\frac{ds}{dt} = -Br_m s \qquad B = 4\pi N\rho_L\left[\frac{R'T}{\xi e_s(T)} + \frac{\varepsilon L_h^2}{pTc_p}\right] \cdot \frac{1}{\left[\left(\frac{L_h}{R_vT} - 1\right)\frac{L_h\rho_L}{KT} + \frac{\rho_L R_v T}{De_s(T)}\right]}, \tag{B5}$$

where L_h is latent heat, R_v is individual gas constant for water vapor, T is air temperature, ρ_L is density of liquid water, K is coefficient of thermal conductivity of air, D is coefficient of diffusion of water vapor in air, e_s (T) is saturation vapor pressure over a plane water surface at temperature T, N is number concentration of droplets, R' is individual gas constant for dry air, $\xi = R'/R_v$, p is air pressure, and c_p is specific heat with pressure held constant.

[42] **Acknowledgments.** We are grateful to Mike Poellot, Tony Grainger, and Andrea Neumann at the University of North Dakota for providing the data and calculation of the dissipation rate; we also thank Seong Soo Yum at the Yonsei University for many helpful discussions on this manuscript. C. Lu and Y. Liu are supported by the DOE Earth System Modeling (ESM) program via the FASTER project (www.bnl.gov/esm) and Atmospheric System Research (ASR) program. S. Niu is supported by the National Natural Science Foundation of China (grants 40537034 and 40775012) and the Qing-Lan Project for Cloud-Fog-Precipitation-Aerosol Study in Jiangsu Province, China.

References

Andrejczuk, M., W. W. Grabowski, S. P. Maltnowski, and P. K. Smolarkiewicz (2004), Numerical simulation of cloud-clear air interfacial mixing, *J. Atmos. Sci.*, *61*, 1726–1739, doi:10.1175/1520-0469(2004)061<1726:NSOCAI>2.0.CO;2.

Andrejczuk, M., W. W. Grabowski, S. P. Malinowski, and P. K. Smolarkiewicz (2009), Numerical simulation of cloud–clear air interfacial mixing: Homogeneous versus inhomogeneous mixing, *J. Atmos. Sci.*, *66*, 2493–2500, doi:10.1175/2009JAS2956.1.

Baker, M. B., and J. Latham (1979), The evolution of droplet spectra and the rate of production of embryonic raindrops in small cumulus clouds, *J. Atmos. Sci.*, *36*, 1612–1615, doi:10.1175/1520-0469(1979)036<1612:TEODSA>2.0.CO;2.

Baker, M. B., R. G. Corbin, and J. Latham (1980), The influence of entrainment on the evolution of cloud droplet spectra: I. A model of inhomogeneous mixing, *Q. J. R. Meteorol. Soc.*, *106*(449), 581–598, doi:10.1002/qj.49710644914.

Baker, M. B., R. E. Breidenthal, T. W. Choularton, and J. Latham (1984), The effects of turbulent mixing in clouds, *J. Atmos. Sci.*, *41*, 299–304, doi:10.1175/1520-0469(1984)041<0299:TEOTMI>2.0.CO;2.

Baumgardner, D. (1987), Corrections for the response times of particle measuring probes, paper presented at the Sixth Symposium on Meteorological Observations and Instrumentation, Am. Meteorol. Soc., New Orleans, La.

Baumgardner, D., and M. Spowart (1990), Evaluation of the forward scattering spectrometer probe. Part III: Time response and laser inhomogeneity limitations, *J. Atmos. Oceanic Technol.*, *7*(5), 666–672, doi:10.1175/1520-0426(1990)007<0666:EOTFSS>2.0.CO;2.

Baumgardner, D., W. Strapp, and J. Dye (1985), Evaluation of the forward scattering spectrometer probe. Part II: Corrections for coincidence and dead-time losses, *J. Atmos. Oceanic Technol.*, *2*(4), 626–632, doi:10.1175/1520-0426(1985)002<0626:EOTFSS>2.0.CO;2.

Bony, S., and J.-L. Dufresne (2005), Marine boundary layer clouds at the heart of tropical cloud feedback uncertainties in climate models, *Geophys. Res. Lett.*, *32*, L20806, doi:10.1029/2005GL023851.

Burnet, F., and J. L. Brenguier (2007), Observational study of the entrainment-mixing process in warm convective clouds, *J. Atmos. Sci.*, *64*, 1995–2011, doi:10.1175/JAS3928.1.

Cess, R. D., et al. (1989), Interpretation of cloud-climate feedback as produced by 14 atmospheric general circulation models, *Science*, *245*(4917), 513–516, doi:10.1126/science.245.4917.513.

Cho, J. Y. N., R. E. Newell, B. E. Anderson, J. D. W. Barrick, and K. L. Thornhill (2003), Characterizations of tropospheric turbulence and stability layers from aircraft observations, *J. Geophys. Res.*, *108*(D20), 8784, doi:10.1029/2002JD002820.

Chosson, F., J.-L. Brenguier, and L. Schüller (2007), Entrainment-mixing and radiative transfer simulation in boundary layer clouds, *J. Atmos. Sci.*, *64*, 2670–2682, doi:10.1175/JAS3975.1.

Colman, R. (2003), A comparison of climate feedbacks in general circulation models, *Clim. Dyn.*, *20*(7), 865–873.

Davis, A. B., A. Marshak, H. Gerber, and W. J. Wiscombe (1999), Horizontal structure of marine boundary layer clouds from centimeter to kilometer scales, *J. Geophys. Res.*, *104*(D6), 6123–6144, doi:10.1029/1998JD200078.

Deng, Z., C. Zhao, Q. Zhang, M. Huang, and X. Ma (2009), Statistical analysis of microphysical properties and the parameterization of effective radius of warm clouds in Beijing area, *Atmos. Res.*, *93*(4), 888–896, doi:10.1016/j.atmosres.2009.04.011.

Dong, X., P. Minnis, G. G. Mace, W. L. Smith, M. Poellot, R. T. Marchand, and A. D. Rapp (2002), Comparison of stratus cloud properties deduced from surface, GOES, and aircraft data during the March 2000 ARM cloud IOP, *J. Atmos. Sci.*, *59*, 3265–3284, doi:10.1175/1520-0469(2002)059<3265:COSCPD>2.0.CO;2.

Dye, J., and D. Baumgardner (1984), Evaluation of the forward scattering spectrometer probe. Part I: Electronic and optical studies, *J. Atmos. Oceanic Technol.*, *1*(4), 329–344, doi:10.1175/1520-0426(1984)001<0329:EOTFSS>2.0.CO;2.

Gerber, H. E., G. M. Frick, J. B. Jensen, and J. G. Hudson (2008), Entrainment, mixing, and microphysics in trade-wind cumulus, *J. Meteorol. Soc. Jpn.*, *86A*, 87–106, doi:10.2151/jmsj.86A.87.

Grabowski, W. W. (2006), Indirect impact of atmospheric aerosols in idealized simulations of convective-radiative quasi equilibrium, *J. Clim.*, *19*(18), 4664–4682, doi:10.1175/JCLI3857.1.

Grabowski, W. W., and H. Pawlowska (1993), Entrainment and mixing in clouds: The Paluch mixing diagram revisited, *J. Appl. Meteorol.*, *32*(11),

1767–1773, doi:10.1175/1520-0450(1993)032<1767:EAMICT>2.0.CO;2.
Gultepe, I., and D. O'C. Starr (1995), Dynamical structure and turbulence in cirrus clouds: Aircraft observations during FIRE, *J. Atmos. Sci.*, *52*, 4159–4182, doi:10.1175/1520-0469(1995)052<4159:DSATIC>2.0.CO;2.
Haman, K. E., S. P. Malinowski, M. J. Kurowski, H. Gerber, and J.-L. Brenguier (2007), Small scale mixing processes at the top of a marine stratocumulus: A case study, *Q. J. R. Meteorol. Soc.*, *133*(622), 213–226, doi:10.1002/qj.5.
Hudson, J. G., and S. S. Yum (1997), Droplet spectral broadening in marine stratus, *J. Atmos. Sci.*, *54*, 2642–2654, doi:10.1175/1520-0469(1997)054<2642:DSBIMS>2.0.CO;2.
Jeffery, C. A. (2007), Inhomogeneous cloud evaporation, invariance, and Damköhler number, *J. Geophys. Res.*, *112*, D24S21, doi:10.1029/2007JD008789.
Jensen, J. B., P. H. Austin, M. B. Baker, and A. M. Blyth (1985), Turbulent mixing, spectral evolution and dynamics in a warm cumulus cloud, *J. Atmos. Sci.*, *42*, 173–192, doi:10.1175/1520-0469(1985)042<0173:TMSEAD>2.0.CO;2.
Khelif, D., S. P. Burns, and C. A. Friehe (1999), Improved wind measurements on research aircraft, *J. Atmos. Oceanic Technol.*, *16*(7), 860–875, doi:10.1175/1520-0426(1999)016<0860:IWMORA>2.0.CO;2.
Kim, B.-G., M. A. Miller, S. E. Schwartz, Y. Liu, and Q. Min (2008), The role of adiabaticity in the aerosol first indirect effect, *J. Geophys. Res.*, *113*, D05210, doi:10.1029/2007JD008961.
Kostinski, A. B., and R. A. Shaw (2001), Scale-dependent droplet clustering in turbulent clouds, *J. Fluid Mech.*, *434*, 389–398, doi:10.1017/S0022112001004001.
Krueger, S. K. (1993), Linear eddy modeling of entrainment and mixing in stratus clouds, *J. Atmos. Sci.*, *50*, 3078–3090, doi:10.1175/1520-0469(1993)050<3078:LEMOEA>2.0.CO;2.
Krueger, S. K. (2008), Fine-scale modeling of entrainment and mixing of cloudy and clear air, paper presented at the 15th International Conference on Clouds and Precipitation, Int. Comm. on Clouds and Precip., Cancun, Mexico.
Labitt, M. (1981), Coordinated radar and aircraft observations of turbulence, *Proj. Rep. ATC-108*, Lincoln Lab., Mass. Inst. of Technol., Cambridge.
Lasher-Trapp, S. G., W. A. Cooper, and A. M. Blyth (2005), Broadening of droplet size distributions from entrainment and mixing in a cumulus cloud, *Q. J. R. Meteorol. Soc.*, *131*(605), 195–220, doi:10.1256/qj.03.199.
Lehmann, K., H. Siebert, and R. A. Shaw (2009), Homogeneous and inhomogeneous mixing in cumulus clouds: dependence on local turbulence structure, *J. Atmos. Sci.*, *66*, 3641–3659, doi:10.1175/2009JAS3012.1.
Lewellen, D. C., and W. S. Lewellen (1998), Large-eddy boundary layer entrainment, *J. Atmos. Sci.*, *55*, 2645–2665, doi:10.1175/1520-0469(1998)055<2645:LEBLE>2.0.CO;2.
Liu, Y., and J. Hallett (1998), On size distributions of cloud droplets growing by condensation: A new conceptual model, *J. Atmos. Sci.*, *55*, 527–536, doi:10.1175/1520-0469(1998)055<0527:OSDOCD>2.0.CO;2.
Liu, Y., P. H. Daum, S. K. Chai, and F. Liu (2002a), Cloud parameterizations, cloud physics, and their connections: An overview, *Recent Res. Dev. Geophys.*, *4*, 119–142.
Liu, Y., P. H. Daum, and J. Hallett (2002b), A generalized systems theory for the effect of varying fluctuations on cloud droplet size distributions, *J. Atmos. Sci.*, *59*, 2279–2290, doi:10.1175/1520-0469(2002)059<2279:AGSTFT>2.0.CO;2.
Lock, A. P. (2001), The numerical representation of entrainment in parameterizations of boundary layer turbulent mixing, *Mon. Weather Rev.*, *129*(5), 1148–1163, doi:10.1175/1520-0493(2001)129<1148:TNROEI>2.0.CO;2.
Malinowski, S. P., and H. Pawlowska (1989), On estimating the entraininent level in cumulus clouds, *J. Atmos. Sci.*, *46*, 2463–2465, doi:10.1175/1520-0469(1989)046<2463:OETELI>2.0.CO;2.
Meischner, P., R. Baumann, H. Holler, and T. Jank (2001), Eddy dissipation rates in thunderstorms estimated by Doppler radar in relation to aircraft in situ measurements, *J. Atmos. Oceanic Technol.*, *18*(10), 1609–1627, doi:10.1175/1520-0426(2001)018<1609:EDRITE>2.0.CO;2.
Paluch, I. R., and D. G. Baumgardner (1989), Entrainment and fine-scale mixing in a continental convective cloud, *J. Atmos. Sci.*, *46*, 261–278, doi:10.1175/1520-0469(1989)046<0261:EAFSMI>2.0.CO;2.
Pawlowska, H., J. L. Brenguier, and F. Burnet (2000), Microphysical properties of stratocumulus clouds, *Atmos. Res.*, *55*(1), 15–33, doi:10.1016/S0169-8095(00)00054-5.
Poellot, M. R., and C. A. Grainger (1991), A comparison of several airborne measures of turbulence, paper presented at the 4th International Conference of the Aviation Weather Systems, Am. Meteorol. Soc., Paris, France.
Rogers, R. R., and M. K. Yau (1989), *A Short Course in Cloud Physics*, Butterworth Heinemann, Burlington, Mass.
Shao, H., and G. Liu (2006), Influence of mixing on evaluation of the aerosol first indirect effect, *Geophys. Res. Lett.*, *33*, L14809, doi:10.1029/2006GL026021.
Siebert, H., H. Franke, K. Lehmann, R. Maser, E. Wei Saw, D. Schell, R. A. Shaw, and M. Wendisch (2006), Probing finescale dynamics and microphysics of clouds with helicopter-borne measurements, *Bull. Am. Meteorol. Soc.*, *87*(12), 1727–1738, doi:10.1175/BAMS-87-12-1727.
Stephens, G. L. (2005), Cloud feedbacks in the climate system: A critical review, *J. Clim.*, *18*(2), 237–273, doi:10.1175/JCLI-3243.1.
Stommel, H. (1947), Entrainment of air into a cumulus cloud, *J. Meteorol.*, *4*(3), 91–94, doi:10.1175/1520-0469(1947)004<0091:EOAIAC>2.0.CO;2.
Su, C.-W., S. K. Krueger, P. A. McMurtry, and P. H. Austin (1998), Linear eddy modeling of droplet spectral evolution during entrainment and mixing in cumulus clouds, *Atmos. Res.*, *47–48*, 41–58, doi:10.1016/S0169-8095(98)00039-8.
Telford, J. W. (1996), Clouds with turbulence; the role of entrainment, *Atmos. Res.*, *40*(2–4), 261–282, doi:10.1016/0169-8095(95)00038-0.
Telford, J. W., and S. K. Chai (1980), A new aspect of condensation theory, *Pure Appl. Geophys.*, *118*(2), 720–742, doi:10.1007/BF01593025.
von Salzen, K., and N. A. McFarlane (2002), Parameterization of the bulk effects of lateral and cloud-top entrainment in transient shallow cumulus clouds, *J. Atmos. Sci.*, *59*, 1405–1430, doi:10.1175/1520-0469(2002)059<1405:POTBEO>2.0.CO;2.
Wang, J., P. H. Daum, S. S. Yum, Y. Liu, G. I. Senum, M.-L. Lu, J. H. Seinfeld, and H. Jonsson (2009), Observations of marine stratocumulus microphysics and implications for processes controlling droplet spectra: Results from the Marine Stratus/Stratocumulus Experiment, *J. Geophys. Res.*, *114*, D18210, doi:10.1029/2008JD011035.
Wyngaard, J. C. (2010), *Turbulence in the Atmosphere*, Cambridge Univ. Press, New York, doi:10.1017/CBO9780511840524.
Yamaguchi, T., and D. A. Randall (2008), Large-eddy simulation of evaporatively driven entrainment in cloud-topped mixed layers, *J. Atmos. Sci.*, *65*, 1481–1504, doi:10.1175/2007JAS2438.1.
Yum, S. S., and J. G. Hudson (2001), Microphysical relationships in warm clouds, *Atmos. Res.*, *57*(2), 81–104, doi:10.1016/S0169-8095(00)00099-5.
Yum, S. S., and J. G. Hudson (2005), Adiabatic predictions and observations of cloud droplet spectral broadness, *Atmos. Res.*, *73*(3–4), 203–223, doi:10.1016/j.atmosres.2004.10.006.
Zhang, Q., J. Quan, X. Tie, M. Huang, and X. Ma (2011), Impact of aerosol particles on cloud formation: Aircraft measurements in China, *Atmos. Environ.*, *45*, 665–672, doi:10.1016/j.atmosenv.2010.10.025.

Y. Liu and C. Lu, Atmospheric Sciences Division, Brookhaven National Laboratory, Bldg. 815E, 75 Rutherford Dr., Upton, NY 11973, USA. (luchunsong110@gmail.com)
S. Niu, School of Atmospheric Physics, Nanjing University of Information Science and Technology, Nanjing, Jiangsu 210044, China.